Multidisciplinary Respiratory Medicine 2023; volume 18:923

pagepress

ORIGINAL RESEARCH ARTICLE

OPEN ACCESS

Experimental studies and mathematical modeling of the viscoelastic rheology of tracheobronchial mucus from respiratory healthy patients

Sandra Melina Tauwald,[1] Johanna Michel,[1] Marie Brandt,[2] Veronika Vielsmeier,[2] Christian Stemmer,[3] Lars Krenkel[1]

[1]Regensburg Center of Health Sciences and Technology, Department of Biofluid Mechanics, University of Applied Sciences (OTH), Regensburg

[2]Department for Otorhinolaryngology, University Hospital Regensburg, Regensburg

[3]Chair of Aerodynamics and Fluid Mechanics, Technical University of Munich (TUM), Munich, Germany

ABSTRACT

Background: Tracheobronchial mucus plays a crucial role in pulmonary function by providing protection against inhaled pathogens. Due to its composition of water, mucins, and other biomolecules, it has a complex viscoelastic rheological behavior. This interplay of both viscous and elastic properties has not been fully described yet. In this study, we characterize the rheology of human mucus using oscillatory and transient tests. Based on the transient tests, we describe the material behavior of mucus under stress and strain loading by mathematical models.

Methods: Mucus samples were collected from clinically used endotracheal tubes. For rheological characterization, oscillatory amplitude-sweep and frequency-sweep tests, and transient creep-recovery and stress-relaxation tests were performed. The results of the transient test were approximated using the Burgers model, the Weibull distribution, and the six-element Maxwell model. The three-dimensional microstructure of the tracheobronchial mucus was visualized using scanning electron microscope imaging.

Results: Amplitude-sweep tests showed storage moduli ranging from 0.1 Pa to 10,000 Pa and a median critical strain of 4%. In frequency-sweep tests, storage and loss moduli increased with frequency, with the median of the storage modulus ranging from 10 Pa to 30 Pa, and the median of the loss modulus from 5 Pa to 14 Pa. The Burgers model approximates the viscoelastic behavior of tracheobronchial mucus during a constant load of stress appropriately (R^2 of 0.99), and the Weibull distribution is suitable to predict the recovery of the sample after the removal of this stress (R^2 of 0.99). The approximation of the stress-relaxation test data by a six-element Maxwell model shows a larger fit error (R^2 of 0.91).

Conclusions: This study provides a detailed description of all process steps of characterizing the rheology of tracheobronchial mucus, including sample collection, microstructure visualization, and rheological investigation. Based on this characterization, we provide mathematical models of the rheological behavior of tracheobronchial mucus. These can now be used to simulate mucus flow in the respiratory system through numerical approaches.

Key words: tracheobronchial mucus; rheological model; viscoelasticity.

Correspondence: Sandra Melina Tauwald, Regensburg Center of Health Sciences and Technology, Department of Biofluid Mechanics, University of Applied Sciences (OTH), Galgenbergstraße 30, 93053 Regensburg, Germany. Tel. +49.941.943.9568. E-mail: melina.tauwald@oth-regensburg.de

Contributions: SMT, LK, performed the measurements; SMT, LK, JM, MB, VV, designed the study; VV, MB, supported the study in terms of medical expertise; SMT, JM, LK, wrote the manuscript in strong consultation with CS. All the authors read and approved the final version of the manuscript and agreed to be accountable for all aspects of the work.

Conflict of interest: All authors certify that they have no affiliations with or involvement in any organization or entity with any financial interest or non-financial interest in the subject matter or materials discussed in this manuscript.

Ethics approval and consent to participate: This study was approved by the Institutional Ethics Commission of Regensburg (No. 22-2979-101). Written consent to participate was obtained from all study participants.
Availability of data and material: the datasets used and/or analyzed during the current study are available from the corresponding author on reasonable request.

Funding: This work is supported by the Regensburg Center of Health Sciences and Technology (RCHST), by the Bavarian Academic Forum (BayWISS), and by the Initiative and Networking Fund of the Helmholtz Association of German Research Centers (HGF) under the CORAERO project (KA1-Co-06).

Introduction

Tracheobronchial mucus, also referred to as airway surface liquid, is a thin liquid layer with a thickness of 5-10 µm [1] that covers the surface of the airways and forms a blanket over the tips of the epithelial cilia [2]. It maintains a strong multifunctional protective barrier between the respiratory epithelia and the gas in the lumen [3,4]. Physiologically, tracheobronchial mucus ensures undisturbed ciliary interaction. Thus, it plays a vital role in protecting the lung from the continuous load of pathogens, particles, and chemicals in the inhaled air [5].

Tracheobronchial mucus mainly consists of water (90-95%), glycoproteins (2-5%), ions (1%), and molecules such as DNA and cell debris [6,7]. It contains two different families of glycoproteins: secreted mucins and cell-tethered mucins. Of these, mainly the secreted polymeric mucins influence mucus rheology [8]. Their chains have a high molecular weight of 200 kDa to 200 MDa and are large in size with diameters from 10 to 300 nm and lengths from 190 to 1500 nm [8,9]. By entangling and cross-linking, these mucins form a complex three dimensional network [6].

The network formed by linked mucins, causes a highly complicated rheological behavior. Mucus is non-Newtonian shear-thinning and non-linear viscoelastic [7,10-12]. Thus, it has properties of both viscous fluids and of elastic solids. Viscosity alone cannot describe this behavior adequately. Further, mucus behaves differently during loading and unloading. Such load changes are intrinsic to the breathing cycle, as the air flow stops and reverses at the end of each inspiration or expiration. Moreover, the reaction of mucus to applied forces, depends on its history of deformation. Strong deformations in the mucus, as they occur in the respiratory system for example during coughing, disrupt the fragile mucin network. This likely changes the flow behavior of the mucus.

These rheological characteristics directly affect the mucus flow [6], which is driven by a combination of mucociliary motion and shear forces exerted by the expiratory airflow [1]. During mucociliary motion, the thin layer of mucus traps pathogens contained in the respiratory air and then removes them by interacting with the cilia. Thus, the mucus layer operates as an indispensable coupler, transferring momentum from the tips of the cilia to the loaded pathogens. This creates mucus movement and thus transports the trapped pathogens. Shear-induced mucus transport, especially during coughing and sneezing, is one of the most important mechanisms in the clearance of potentially pathogen-contaminated tracheobronchial mucus [13] as it leads to aerosol and droplet excretion.

Changes in the amount and in the rheological properties of tracheobronchial mucus play an important pathophysiological role in the severity of symptoms in many respiratory diseases [6,14]. Such pathological changes occur in conditions such as bronchial asthma or cystic fibrosis [6,7]. Further, absence of mucus leads to a lack of particle transport, despite active ciliary motion [15]. Especially, the viscoelastic properties of tracheobronchial mucus affect its flow directly [6].

Both the physiological behavior of mucus and its pathological changes can be better understood with a profound knowledge of its physiological rheology. As such, a rheological characterization of tracheobronchial mucus opens up opportunities to improve both medical diagnosis [16] and treatment methods that use the respiratory mucosa as the application area. Further, a full characterization of the rheology of physiological mucus can build a reference base for pathological changes and provide data for numerical investigations of mucus transport and shear-induced aerosol generation in the upper airways [17,18].

Most recent studies investigated the rheological properties of tracheobronchial mucus, as well as mucus mimetics, only partly [12,19,20]. Oscillatory (investigating storage modulus G' and loss modulus G'') and/or continuous shear investigations (investigating viscosity) characterize only a subset of the complex rheological behavior [6]. However, numerical investigations, which can describe the more complex flow conditions in the human respiratory system based on experimental data from simplified tests on respiratory mucus, as well as the design of mucus simulants require a full characterization of both the viscous and the elastic behavior especially the interplay of these properties. Further, for numerical applications, mathematical models describing the rheological behavior are necessary. Due to the complexity of the mucus rheology, it is not possible to represent mucus behavior during a breathing cycle by a single model. Depending on the problem to be solved, models of the response of the mucus to stress or force loading or to strain or deformation loading, or combinations of these models are necessary.

Such models can be deducted from transient testing. These identify the interplay of viscous and elastic properties over time in simplified flow situations. Stress-relaxation tests investigate the material's response to an applied force, which is induced in the airways for example by coughing. Creep-recovery tests identify the response of the mucus to a defined deformation, which is induced in the airways for example by beating cilia. To derive statistically grounded models from experimental data of transient tests, a high number of investigated samples is necessary.

To collect such high sample numbers of human mucus, previously described tracheobronchial mucus collection methods [21,22] were not applicable. Common sample collection procedures such as the cytology brush method might damage the sample pre-testing via high shear forces. Further, saliva might contaminate the sample during the bronchoscopy. Additionally, an *in vitro* measurement environment does not completely reproduce physiological *in vivo* conditions (23). To overcome these limitations, a novel method to collect sample from endotracheal tubes without high shear forces and saliva contamination was developed within this study.

This project provides a full characterization of physiological, human mucus rheology. First, it describes the reproducible sampling method of collecting physiological, tracheobronchial mucus from endotracheal tubes. The mucus rheology is characterized via oscillatory tests and transient creep-recovery and stress-relaxation tests. Finally, mathematical models of the time-dependent mucus behavior are deducted. These include the Burgers model of stress loading, the Weibull distribution of stress release, and the six-element Maxwell model of stress relaxation. Visualizations of the microstructure of the mucus illustrate how the three-dimensional mucin network determines the complex rheological properties of tracheobronchial mucus.

Materials and Methods

Clinically used endotracheal tubes with adhering samples of tracheobronchial mucus were collected. The rheological behavior of the tracheobronchial mucus was investigated in amplitude-sweep tests, frequency-sweep tests, creep-recovery tests, and stress-relaxation tests. Then, transient test results were approximated by mathematical models: the Burgers model (creep-test), the Weibull model (recovery-test), and the six-element Maxwell model (relaxation-test). The process steps of this study as shown in Figure 1 are described in the following in detail.

Sample collection

Tracheobronchial mucus samples were collected from endotracheal tubes used in surgery by otorhinolaryngology specialists at

the University Hospital Regensburg. For this, anesthesiologists collected the tubes after the patients were extubated. Donors included in the study were over the age of eighteen and did not have any infectious respiratory disease. All donors gave informed consent regarding the biomedical research on tracheobronchial mucus. The institutional ethics commission of Regensburg (No. 22-2979-101) approved the protocol. The tubes were stored for transport in airproof plastic bags at a temperature of 5°C for a maximum of three days before the samples were analyzed.

Microstructure visualization

Images of the sample microstructure were captured with two scanning electron microscopes (SEM) (LEO 1455VP, Carl Zeiss Microscopy GmbH, Oberkochen, Germany; MIRA, Tescan GmbH, Dortmund, Germany). Tracheobronchial mucus has a high content of water. This water needs to be eliminated from the sample before visualization in a SEM. To visualize the cross-linked glycoproteins, which determine mucus's rheological behavior, the drying process needs to preserve the spatial structure of the mucus. To achieve this, mucus samples were pre-treated by freeze drying. A small amount of mucus of 1 g was freeze-dried over two days, using a vacuum of 0.31 mbar and a temperature of -6°C (Beta 1-8K, Martin Christ, Osterrode am Harz, Germany). To minimize loading of the sample and thus overexposure during high magnification in the MIRA SEM, these samples were gold-sputtered (coating thickness 5 nm) before scanning.

Rheological investigation

Before the rheological investigations, the integrity of each sample was assessed. For this, the tubes were investigated optically to ensure a sufficient mucus sample volume and to rule out blood contamination. A completely filled gap between cone geometry and peltier element defines a sufficient mucus sample (approximately 100 µL). Tubes with insufficient mucus volume, heterogenous mucus abnormalities or contamination were discarded.

The rheometer's (Discovery HR 30, TA Instruments, New Castle, DE, USA) inertia and friction were calibrated before each measurement sequence, which lasted a maximum of six hours and included three to eight samples. All measurements were performed on a cone-plate geometry with a cone angle of one degree and a cone base diameter of 20 mm. Samples were prepared according to the process illustrated in Figure 2. First, samples were carefully transferred from the endotracheal tubes to the temperature-controlled plate (Peltier element) of the rheometer using a spatula (Figure 2 A,B). Then, the upper cone was lowered to a truncation gap of 40 µm above the peltier element. Any sample protruding the measurement area was carefully removed (Figure 2C). Subsequently, the upper cone was lowered to the final measurement gap size of 20 µm between the tip of the cone and the peltier element. A low viscous silicone oil (5cSt, Carl Roth GmbH, Karlsruhe, Germany) was applied to the perimetral boundaries of the cone to prevent the sample from evaporating by sealing during the measuring procedure (Figure 2D). To simulate physiological conditions, the measuring temperature was set to 37°C with a tem-

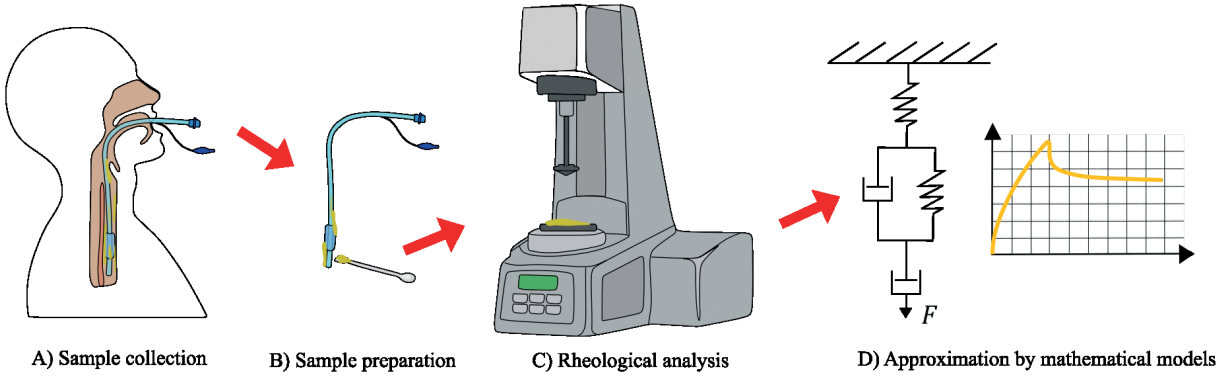

Figure 1. Overview of the study's methods. A) Sample collection; B) sample preparation; C) rheological analysis; D) approximation of experimental data with mathematical models.

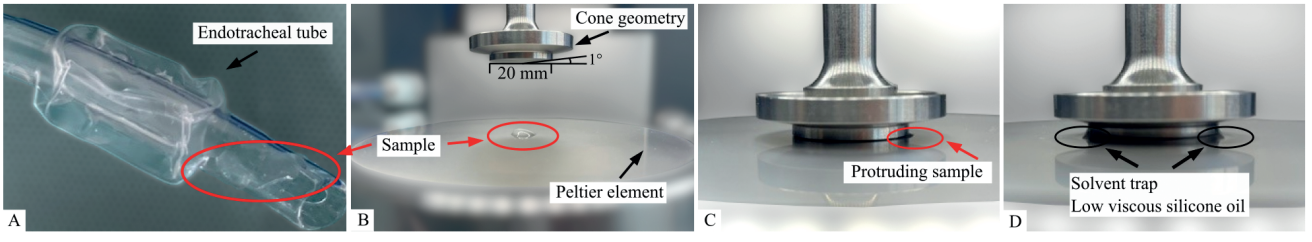

Figure 2. Rheological analysis. A) Sample collection from endotracheal tubes; B) rheometer setup with cone geometry and the sample loaded onto the Peltier element; C) sample protrudes once the cone is lowered; D) a solvent trap covers the sample during the measurement.

perature control system. In order to achieve a homogenous temperature throughout the sample, each sample was preheated for 180 seconds before the measurement.

In total four different rheological tests, which can be separated into two groups, were conducted: oscillatory tests and transient tests. The oscillatory tests include amplitude-sweep and a frequency-sweep tests. Transient tests were conducted as creep-recovery and stress-relaxation tests. Each rheological test was performed with a sample size of at least 20 subjects. Table 1 shows the number of investigated samples for each test. Due to the small volume of adhering mucus, only one sample was extracted per endotracheal tube. Only a single test was possible for each sample because the influence of the testing on rheological properties is unknown. In total 97 samples were measured in the rheological tests.

All measured quantities were first analyzed within TRIOS software (Version 5.1, TA Instruments, New Castle, United States). Subsequent statistical analysis and mathematical model fitting was performed using the MATLAB software (R2022b, Mathworks, Carlsbad, CA, USA). To fully characterize the rheological behavior of tracheobronchial mucus, four consecutive tests were conducted. Each test determines a different property: the amplitude-sweep test (Figure 3A) identifies the maximum applicable force, in which the applied strain does not disrupt the fragile microstructure. The frequency-sweep test (Figure 3B) provides a basic characterization whether viscous or elastic behavior is predominant. The creep-recovery test gives information of the interplaying viscous and elastic behavior at a defined deformation of the sample over time (Figure 3C). In addition, the stress-relaxation test (Figure 3D) provides information about the rheological behavior of a sample loaded with a defined force to complete the full characterization of the rheological behavior of tracheobronchial mucus. In the following, the tests and their parameters are described in detail.

Oscillatory tests

Oscillatory tests impose cyclically oscillating strain on a sample. The viscous as well as the elastic properties of the sample can be investigated. Within amplitude-sweep tests, the strain amplitude of a constant-frequency oscillation is gradually increased. This allows for the identification of a linear viscoelastic region (LVR). The frequency-sweep test investigates the stress induced in the sample by an oscillation with a strain amplitude within the LVR and varying frequencies.

Amplitude-sweep tests

The LVR is the region of applied strain in which the sample retains its microstructural properties. In the LVR, the shear moduli are constant and independent of the applied strain. The critical strain marks the limit of the LVR. Once the applied strain exceeds the critical strain, the structural properties of the sample are irreversibly destroyed. A correlation between structural properties and viscoelastic behavior is no longer possible. Thus, combinations of elasticity and viscosity laws based on Newton and Hook are no longer valid. To identify the bounds of the LVR, an amplitude-

Table 1. Breakdown of the collected tubes and measured samples in the rheological tests.

Rheological test	Number of samples
Amplitude-sweep test	21
Frequency-sweep test	36
Creep-recovery test	20
Stress-relaxation test	20
Total tubes collected	*179*
Total samples analyzed	*97*

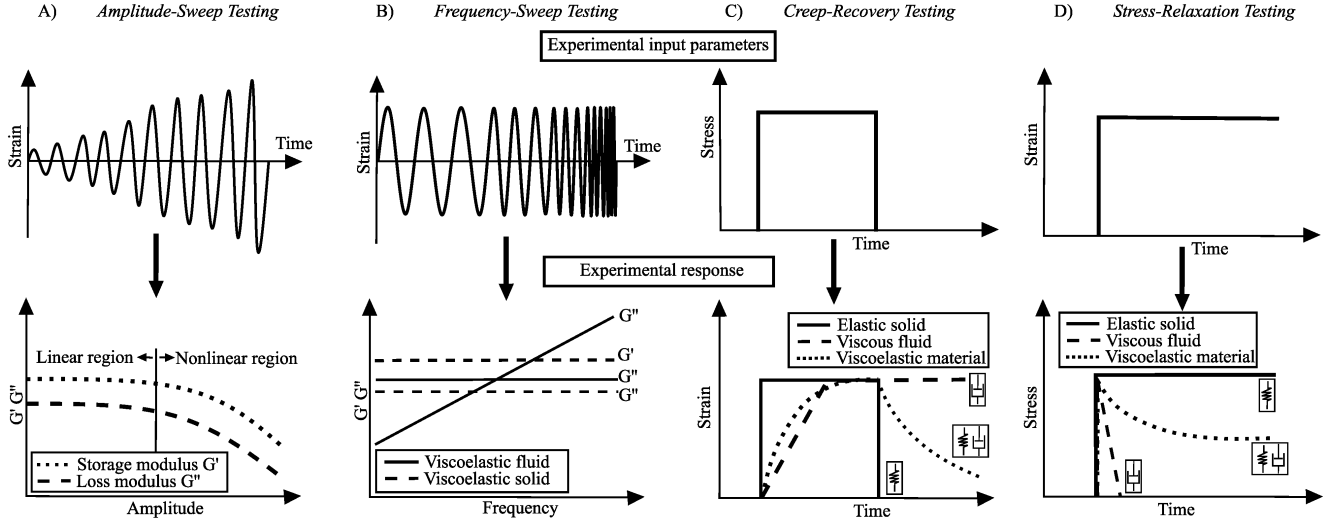

Figure 3. Schematic of the experimental input and output of an amplitude-sweep test (A), a frequency-sweep test (B), a creep-recovery test (C) and a stress-relaxation test (D). Exemplary behavior of storage and loss moduli is given for the oscillatory tests. For the transient tests, the experimental response of an elastic solid, a viscous fluid and a viscoelastic material is given.

sweep test was performed. For this, the sample was tested at a constant oscillation frequency of 10 rad/s and a varying oscillation strain amplitude ranging from 0.01% to 200%. The storage modulus G' was monitored with a sampling rate of 5 points per oscillation strain amplitude decade (0.1-1%, 1-10%, 10-100%, 100-1000%). Subsequently, the critical strain was identified as the strain value at which the storage modulus falls beneath its constant plateau for more than 10% of the plateau value. For each of the 21 samples, the critical strain was evaluated. Then, the averaged critical strain was assumed at the median of the individual critical strain values.

Frequency-sweep tests

Based on the averaged critical strain identified in the amplitude-sweep test, a strain amplitude of 2% was set for the frequency-sweep tests. The angular frequency was varied from 0.08 rad/sec to 100 rad/sec. Both the storage modulus G' and the loss modulus G'' were recorded with a sampling rate of 5 points per decade of the angular frequency (0.1-1 rad/sec, 1-10 rad/sec, 10-100 rad/sec). For each angular frequency, the medians of the storage and loss modulus were calculated to represent the frequency-dependent behavior of the mucus. As such, the storage modulus quantifies its elastic properties, while the loss modulus quantifies its viscous properties. The schematic of a frequency-sweep test in Figure 3B shows an exemplary behavior of a viscoelastic fluid and a viscoelastic solid.

Transient tests

Transient tests measure the time-dependent behavior of the mucus. For this, a constant load is applied to the sample, held for a specific time and released again. The time-dependent response of the sample after the load changes is measured. The type of load determines which quantities are measured. In creep-recovery testing, a constant shear stress is applied, and the strain response is measured. In stress-relaxation testing, a constant strain is applied and the induced stress is measured [24]. The schematic of transient tests in Figure 3 C,D shows the exemplary rheological behavior of a pure viscous material, an ideal elastic material, and a viscoelastic material. It includes the materials' responses to a strain load during stress-relaxation testing and to a stress load during creep-recovery testing. The critical stress, which limits the LVR, is not equivalent in oscillatory and transient tests. Thus, preliminary tests for determining the LVR for the transient tests were performed. To identify the critical stress in creep-recovery tests, and respectively the critical strain in stress-relaxation tests, the compliance curves of repeating transient tests with increasing stress/strain applications were analyzed. If the applied stress/strain is located within the LVR, the compliance curves overlap nearly. Loads exceeding the LVR cause the compliance curves to differ significantly. In the following, the measuring protocols for the creep-recovery test and the stress-relaxation test are presented.

Creep-recovery tests

Creep-recovery tests can be separated into two parts: the loading part (creep part) and the recovery part. The creep part involved loading a sample with a constant stress of 5 Pa for 300 s. The achieved deformation (strain) of the sample was monitored. To account for faster processes at the onset of the loading, a logarithmically increasing temporal sampling interval starting at 100 µs was used. Over a time of 300 s, the degree of elastic deformation and the rate of viscous flow was analyzed. During the relaxation phase, the stress load on the sample was removed, and the total recoverable elastic deformation was analyzed by monitoring the time-dependent strain $\varepsilon(t)$ over a time of 600 s. Again, a logarithmically increasing sampling interval starting at 100 µs was used.

Stress-relaxation tests

In the stress-relaxation tests, a constant strain of 10% was applied to the sample. The deformation was kept constant for the measuring time of 300 sec during which the stress reaction was measured. Due to the mucus's viscoelastic properties, the sample creeped, and the measured stress decreased.

Mathematical characterization of transient tests

From the individual sample response curves of the transient tests, a median was calculated for each measured timestep to deduct average curves for the creep, recovery, and relaxation behavior of physiological tracheobronchial mucus. Mathematical models were fitted to the median data using a non-linear least square fit. In the following sections, the mathematical models for approximating the transient behavior are explained.

Mathematical modelling of creep-recovery tests

The viscoelastic behavior of a material can be modeled with a combination of springs and dashpots. Thereby, a dashpot represents a purely viscous sample. A spring models an ideal elastic material. With its spring constant E and the loaded stress σ_0, the strain ε of a spring follows Hooke's law:

Dashpots have Newtonian behavior. Thus, their strain rate $\dot{\varepsilon}$ results from the fluid's viscosity η, the loaded stress σ_0 and the time t since the load application:

$$\varepsilon(t) = \frac{\sigma_0}{E}. \quad \text{(eq.1)}$$

$$\dot{\varepsilon}(t) = t\,\frac{\sigma_0}{\eta}. \quad \text{(eq.2)}$$

The serial combination of one spring and one dashpot is called a Maxwell element (eq. 3). Its rheological parameters are the spring constant E_M and the dashpot viscosity η_M .

$$\varepsilon(t) = \sigma_0 \cdot \left(\frac{1}{E_M} + \frac{t}{\eta_M}\right). \quad \text{(eq.3)}$$

The parallel combination of one spring with one dashpot results in a so-called Kelvin element (eq.4). Its rheological parameters are the spring constant E_k and the dashpot viscosity η_K.

$$\varepsilon(t) = \frac{\sigma_0}{E_K} \cdot \left(1 - e^{\frac{E_K \cdot t}{\eta_K}}\right). \quad \text{(eq.4)}$$

The time-dependent strain $\varepsilon(t)$ during the creep phase can be described by a combination of a Maxwell and a Kelvin element in series (eq. 5) which is then called the Burgers model [25].

$$\varepsilon(t) = \sigma_0 \cdot \left(\frac{1}{E_M} + \frac{t}{\eta_M} + \frac{1}{E_K} \cdot \left(1 - e^{\frac{-E_K}{\eta_K} t}\right)\right). \quad \text{(eq.5)}$$

The rheological behavior during the recovery phase after the load removal can be approximated by a Weibull distribution (Eq.6 (26, 27)). Thereby, the time-dependent strain $\varepsilon(t)$ is described by the viscoelastic strain recovery ε_{ve}, the scale parameter η_r, and the shape parameter β_r. ε_∞ is the permanent strain remaining after the load removal, which is caused by viscous effects.

$$\varepsilon(t) = \varepsilon_{ve} \cdot e^{\left(-\left(\frac{t}{\eta_r}\right)^{\beta_r}\right)} + \varepsilon_\infty. \quad \text{(eq.6)}$$

Mathematical modelling of stress-relaxation tests

The time-dependent stress response $\sigma(t)$ to the continuous strain load ε can be expressed by a six-element Maxwell model, which is composed of three Maxwell elements combined in parallel (eq. 7) [28]. Thereby, σ_0 describes the initial stress caused by the constant strain at $t = t_0 = 0$ s.

$$\sigma(t) = \sigma_0 \cdot \left(e^{\frac{(-t-t_0)\cdot E_{M1}}{\eta_{M1}}} + e^{\frac{(-t-t_0)\cdot E_{M2}}{\eta_{M2}}} + e^{\frac{(-t-t_0)\cdot E_{M3}}{\eta_{M3}}} \right). \quad \text{(eq.7)}$$

The rheological constants of the six-element Maxwell model are the spring constants E_{M1}, E_{M2}, and E_{M3} and the dashpot viscosities η_{M1}, η_{M2}, and η_{M3}.

Results

In total 97 out of the 179 collected endotracheal tubes were measured in the rheological investigations (Table 1). They contained a sufficient volume of homogenous sample for non-destructive sample collection and showed no contamination. The eliminated tubes were contaminated by blood, had a heterogeneous composition, or contained an insufficient sample amount. Others were used for preliminary tests, to adjust measurement parameters such as investigated shear rates. The freeze-drying preparing the samples for SEM caused a sample weight loss of 83%. Figure 4 A,B show the foamy, three-dimensional structure of the tracheobronchial mucus's matrix spanned by glycoproteins in the non-sputtered samples. The protein fibers crosslink uncoordinatedly. In addition, cuticles are visible, which also crosslink three-dimensionally. Figure 4 C,D show the thin fibers of the glycoprotein network with a diameter of 180-450 nm as well as disrupted structures. The amplitude-sweep test was conducted on 21 samples to identify their LVRs. Once the applied strain amplitude exceeds the sample's critical strain, the sample's storage modulus G' decreases significantly. Figure 5 shows the response of the samples' storage moduli G' to an oscillating strain with amplitudes reaching from 0.01% to 200% at a constant frequency of 10 rad/s. The storage moduli range from 0.1 Pa to 10,000 Pa. The critical strain of each analyzed sample is derived from the point where the sample's storage modulus G' falls below its plateau value for more than 10%. The median of all samples' critical strain values is located at an

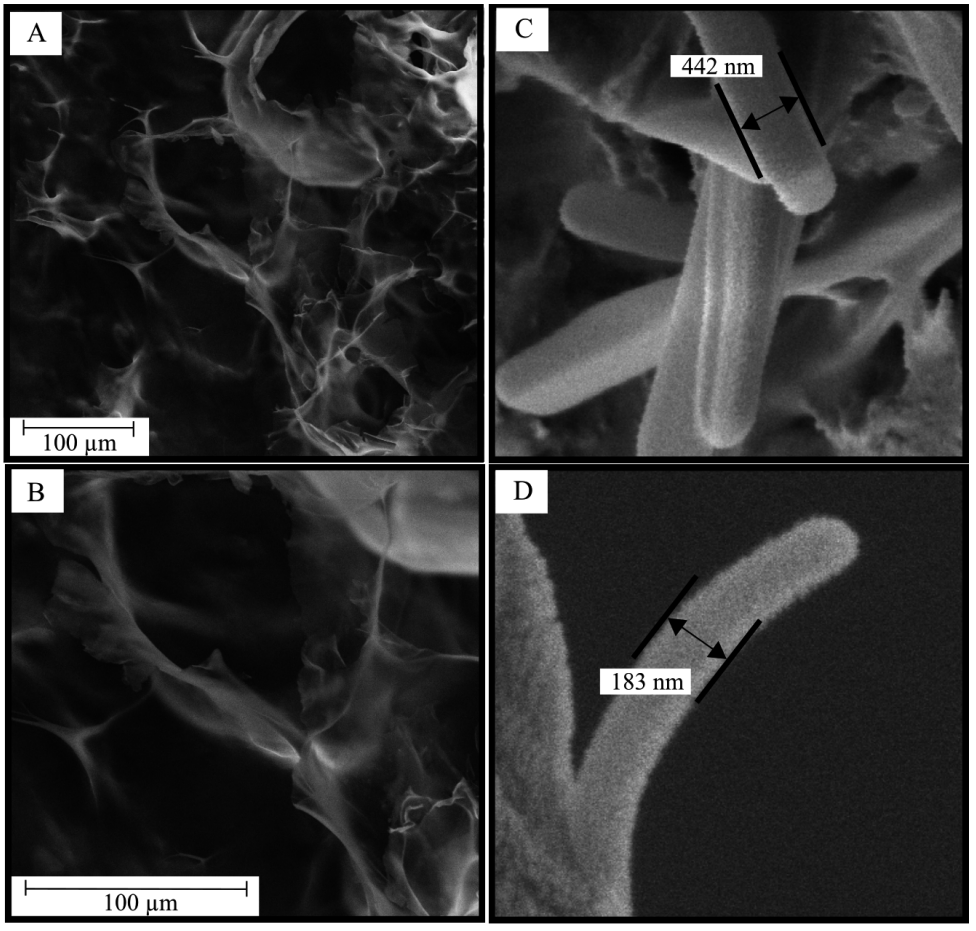

Figure 4. Scanning electron microscopic analysis of freeze-dried tracheobronchial mucus. A,B) Non-sputtered sample in a lower magnification to visualize the three-dimensional foamy microstructure; C,D) gold-sputtered sample in a higher magnification to show single fibers.

oscillation strain amplitude of 4%. The interquartile range (IQR) of the samples' critical strains reaches from 0.6% to 6.3%. The whiskers indicate the 1.5 x IQR and span a distance from 0.17% to 25.1%. The frequency-sweep test enabled to separate viscous and elastic properties of tracheobronchial mucus. Throughout all measured frequencies, the median of the elastic storage modulus was higher than the median of the viscous loss modulus at the same frequency. The strain amplitude for the frequency-sweep test was set to 2% to ensure measurements in the LVR. Figure 6 shows the frequency dependence of the storage modulus G' (Figure 6 left) and the loss modulus G" (Figure 6 right) of 36 tracheobronchial mucus samples. In both figures, the colored crosses represent the moduli of each sample at the measured frequencies. The red line connects the medians of the moduli at each measured frequency. Values exceeding 1.5 x IQR are marked as outliers and are shown as circles. Both the storage and the loss modulus increase with increasing frequency. The median of the storage modulus starts at 10 Pa at 0.08 rad/s and increases to 30 Pa at 100 rad/s. The median of the

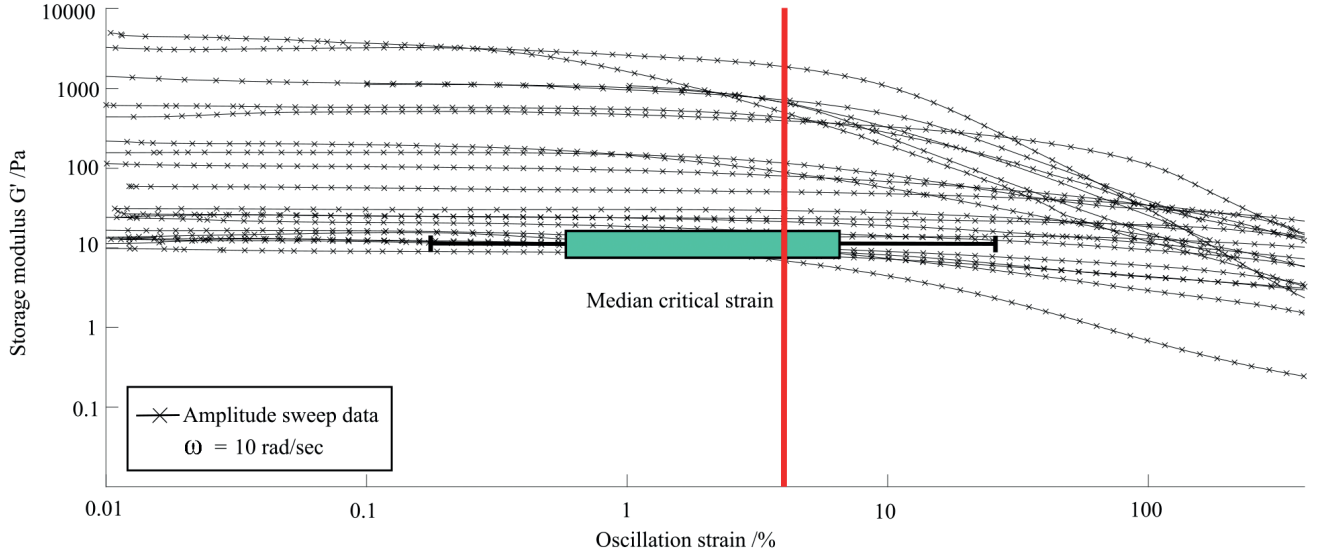

Figure 5. Amplitude-sweep test results: storage modulus G' plotted over the oscillation strain amplitude. The black crosses indicate the experimental data. The red line marks the median critical strain. The green box shows the critical strain interquartile range (IQR). The whiskers indicate the 1.5 x IQR.

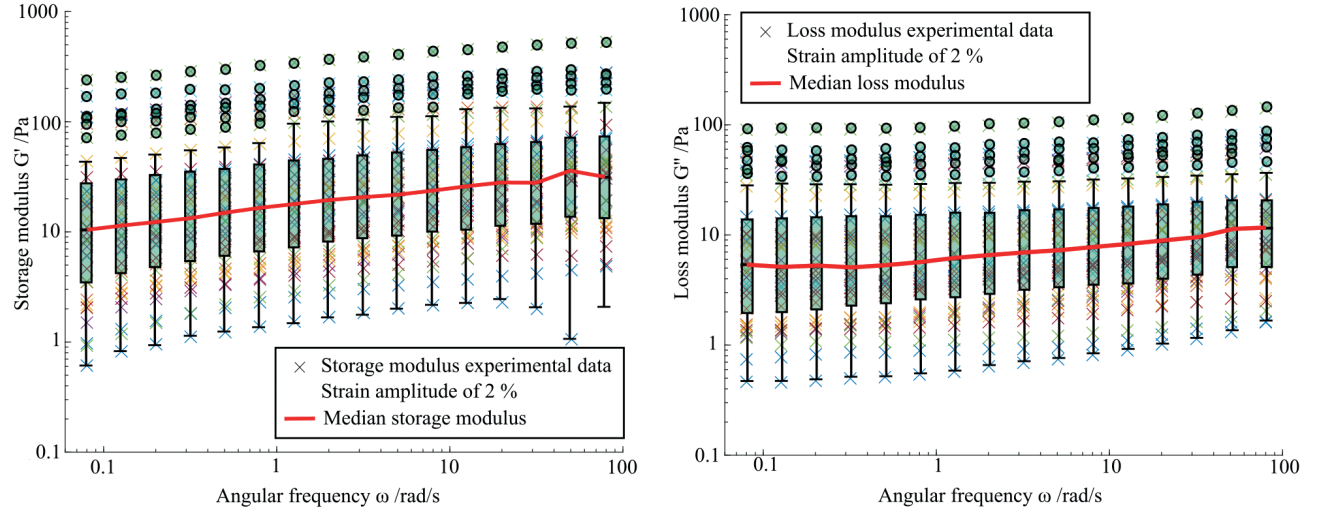

Figure 6. Frequency-sweep test results: storage G' and loss modulus G'' plotted over time. The crosses indicate the experimental data, while the red line shows the median of the data for the investigated frequencies.

loss modulus has lower values, starting at 5 Pa and ending at 14 Pa. The combination of viscous and elastic properties determines the time dependent behavior of the mucus. Transient testing (creep-recovery test, stress-relaxation test) can characterize this interplay over time. In the following, the results of the transient tests are presented. Mathematical model parameters for optimal approximations to the experimental data are presented in Tables 2 to 4. The creep curves of all samples showed a marked increase after the onset of loading. With time, the strain increase rates of all samples declined. A lower increase at the beginning led to an even lower increase rate after longer time, in the extreme to a nearly steady strain. Figure 7 shows the time-dependent strain during the creep part of the creep-recovery tests of 20 samples. The consecutive black crosses indicate the chronological strain sequence of each sample, after loading with a constant stress of 5 Pa. The resulting high gradients are well resolved by the high sampling rate at the beginning of the measurement. The red line connects the median of the strain of all samples at each time step. Two samples showed significantly higher strain exceeding 20 and were identified as outliers. The variance of the sample data is shown at every 15th time step with boxplots. The creep behavior of each sample was mathematically represented by the Burgers model. The black lines show the transient strain values predicted by an individual model for each sample. Across all individual models of the samples, the mean approximation coefficient of determination R^2 is 0.99. A Burgers model fitted to the median strains of all samples at each time step achieves an R^2 of 0.99. Table 2 shows the median Burgers model coefficients with 95% confidence intervals. The spring constant of the Maxwell element E_M resulted in 29 Pa and the dashpot constant of the Maxwell element η_M resulted in 695.3 Pa s. The spring constant of the Kelvin element E_K resulted in 7.179 Pa and the dashpot constant of the Kelvin element η_K resulted in 108 Pa s. The recovery curves of all samples showed a marked strain decrease during the first seconds. With time, the strain stabilized to a constant value. The time-dependent strains of the 20 samples during the recovery part of the creep-recovery test, after the continuous load of 5 Pa was lifted from the sample, are shown in Figure 8 over the measuring time of 600 sec. The black crosses indicate the strain recovery sequence for each sample over time. The two outliers identified in the creep part of the creep-recovery test persist in the recovery data. The variance of the sample data is shown at every 15th time step with boxplots in Figure 8. The recovery behavior of each sample was mathematically represented by the Weibull distribution. The black lines show the data predicted for each sample by a Weibull distribution fitted to the strain data of each sample. The individual fits have an average R^2

Table 2. Coefficients (in *italics*) of the Burgers model fitted to the medians of the experimental data of the creep part of the creep-recovery test. The upper and lower limits of the coefficients within a 95% confidence interval are given below.

$$\text{Burgers model: } \varepsilon(t) = \sigma_0 \cdot \left(\frac{1}{E_M} + \frac{t}{\eta_M} + \frac{1}{E_K} \cdot \left(1 - e^{\frac{-E_K}{\eta_K} \cdot t} \right) \right)$$

E_M (Pa)	η_M (Pa s)	E_K (Pa)	η_K (Pa s)
29	*695.3*	*7.179*	*108*
[27.2, 30.8]	[675.1, 715.4]	[6.848, 7.51]	[98.97, 117]

Table 3. Dimensionless coefficients (in *italics*) of the Weibull model fitted to the medians of the experimental data of the recovery part of the creep-recovery test. The upper and lower limits of the coefficients within a 95% confidence interval are given below.

$$\text{Weibull model: } \varepsilon(t) = \varepsilon_{ve} \cdot e^{\left(-\left(\frac{t}{\eta_r}\right)^{\beta r}\right)} + \varepsilon_\infty$$

ε_{ve}	η_r	β_r	ε_∞
333.9	*921.5*	*0.08828*	*333.9*
[301, 366.9]	[-607.8, 2451]	[0.0828, 0.0936]	[301, 366.9]

Table 4. Dimensionless coefficients (in *italics*) of the six-element Maxwell model fitted to the medians of the experimental data of the stress-relaxation test. The upper and lower limits of the coefficients within a 95% confidence interval are given below.

$$\text{Six-element Maxwell model: } \sigma(t) = \sigma_0 \cdot \left(e^{\frac{(-t-t_0)\cdot E_{M1}}{\eta_{M1}}} + e^{\frac{(-t-t_0)\cdot E_{M2}}{\eta_{M2}}} + e^{\frac{(-t-t_0)\cdot E_{M3}}{\eta_{M3}}} \right)$$

σ_0(Pa)	E_{M1}(Pa)	η_{M1} (Pa s)	E_{M2} (Pa)	η_{M2} (Pa s)	E_{M3} (Pa)	η_M3 (Pa s)
1.19	*0.993*	*0.3312*	*0.05594*	*1.758*	*165.2*	*0.5522*
[1.108, 1.272]	[-2.074*10^6, 2.074*10^6]	[0.919*10^5, 6.919*10^5]	[-1.155*10^5, 1.155*10^5]	[-3.63*10^6, 3.63*10^6]	[-3.707*10^8, 3.707*10^8]	[-1.239*10^6, 1.239*10^6]

of 0.99. The red line connects the median strain of all samples at each time step. The fit of a Weibull distribution to the median strain values has an R^2 of 0.99. Table 3 shows the model parameters of the Weibull approximation of the median data. The viscoelastic strain recovery ε_{ve} resulted in a dimensionless value of 333.9, the scale parameter η_r resulted in a dimensionless value of 921.5, the shape parameter β_r resulted in a dimensionless value of 0.08828, and ε_∞ as the permanent strain caused by the viscous effects resulted in a dimensionless value of 333.9.

During the stress relaxation tests, the induced stress decreased markedly within the initial 10 seconds. After this decrease, the remaining stress, hereinafter called equilibrium stress, was nearly constant. Preliminary tests showed that an initially applied larger stress causes a higher equilibrium stress. Figure 9 shows the time-dependent stress during stress-relaxation tests while loading the samples with a constant strain of 10%. Boxplots indicating the IQR of the experimental data are shown for every 10th time step. Two outliers were identified in the stress-relaxation test. These are not visible in the graphic. The median stress of all samples at each timestep is visualized in red. The stress-relaxation behavior of each

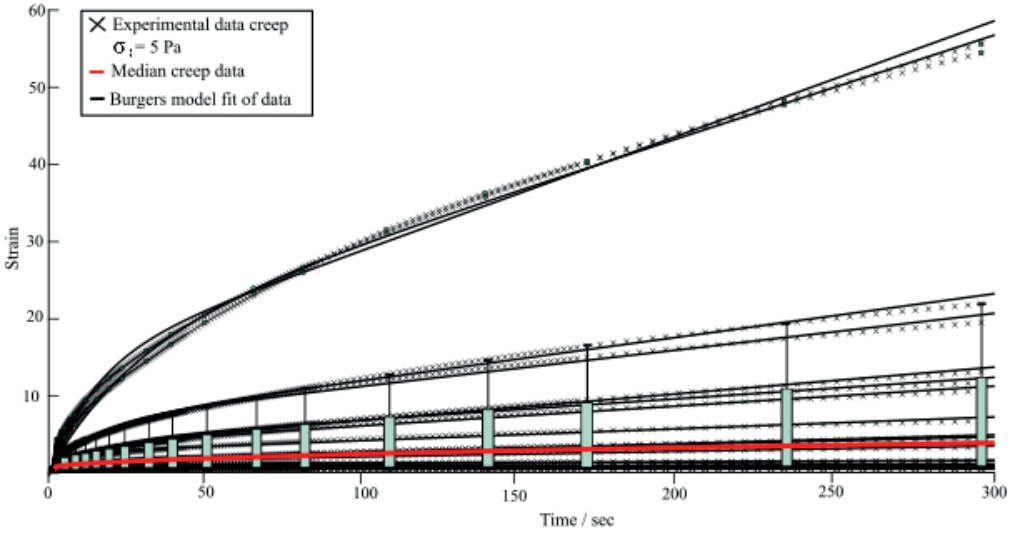

Figure 7. Strain response during the creep part of the creep-recovery test. The black crosses indicate the experimental data, the black lines the approximation by Burgers models fitted to each sample, and the red line connects the median strain values at each timestep.

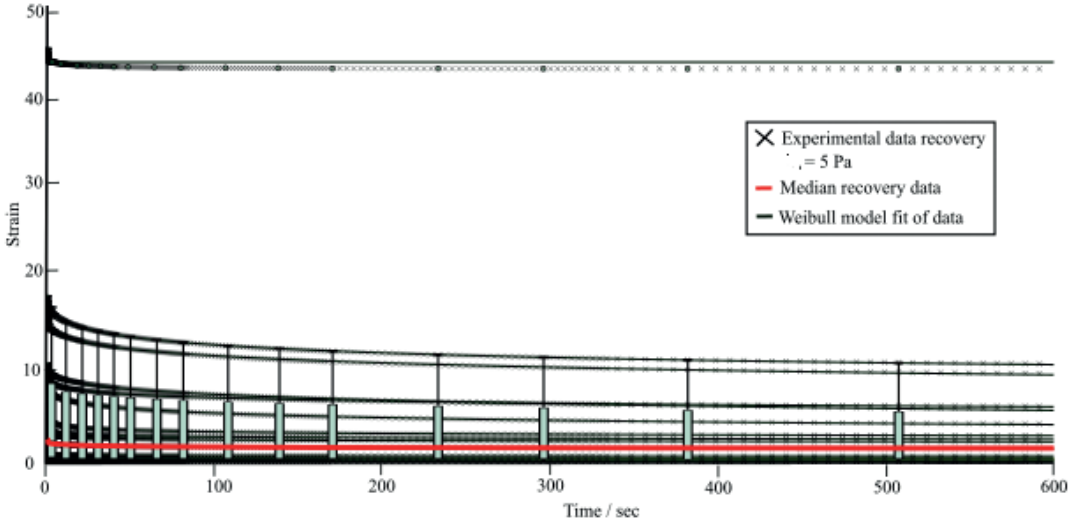

Figure 8. Strain response during the recovery-part of the creep-recovery test. The black crosses indicate the experimental data, the black lines the approximation by Weibull's models fitted to each sample, and the red line connects the median strain values at each timestep.

sample was mathematically represented by the six-element Maxwell model. The stress prediction by a six-element Maxwell model fitted to the median data is shown in green. Table 4 shows the coefficients of this six-element Maxwell model with 95% confidence bounds. The initial stress σ_0 resulted in 1.19 Pa, the spring and the dashpot constants resulted in 0.993 Pa and 0.3312 Pa s for the first Maxwell element, in 0.05594 Pa and 1.758 for Pa s the second Maxwell element, and in 165.2 Pa and 0.5522 Pa s for the third Maxwell element. The fit of the six-element Maxwell model to the median stress values has an R^2 of 0.91.

Discussion

Due to the sensible microstructure of the tracheobronchial mucus and the difficulties of collecting the sample [29], the rheological behavior varies. Thus, a large sample size is necessary to achieve reproducible results regarding the viscoelastic properties of tracheobronchial mucus. This is underlined further by the high ratio of endotracheal tubes that needed to be excluded from the study of nearly 55%. Therefore, the sample collection method potentially affects a high number of patients. Collecting the mucus samples from used endotracheal tubes makes it possible to obtain high sample numbers without any additional impact on patients' wellbeing. Further, this method ensures a defined localization of the collected sample in the trachea. Contamination by saliva can be neglected. Despite the high number of collected endotracheal tubes, the number of samples measured per test is limited. Thus, a pathological characterization of several diseases by mucus rheology requires a larger sample size.

The cross-linked three-dimensional network of glycoproteins in the tracheobronchial mucus could be visualized by SEM with the help of freeze-drying samples preliminarily. The weight loss and the SEM-images showed a successful and gentle freeze-drying process that preserved the three-dimensional microstructure of the mucus. The thin fibers span an unstructured network, which causes the viscoelastic behavior. The application of a small load causes the fibers to arrange in the strain direction. The critical strain marks the strain at which the fibers are fully aligned. Any additional deformation breaks the fibers, which renders the deformation non-reversible.

The complex viscoelastic behavior of tracheobronchial mucus results primarily from the cross-linking by covalent and non-covalent bonds between the macromolecules [20]. Within oscillation tests, this behavior can be modeled with a combination of the mucus storage G' und loss modulus G'', the complex modulus [30]. The validity of the complex modulus is limited to the LVR. Therefore, knowledge of the mucus's LVR is necessary. All samples showed an LVR in the amplitude-sweep-tests. Once the applied strain exceeds the critical strain, the storage modulus decreases. For the following frequency-sweep oscillatory tests a strain amplitude within the LVR needed to be set. Because of the small sample volume which could be obtained from each endotracheal tube, only one test per sample was possible. Thus, it was not possible to perform both amplitude- and frequency-sweep tests with one sample. The critical strain of each sample measured in the frequency-sweep test was unknown. Therefore, the strain amplitude for the frequency-sweep tests was deducted from the averaged critical strain distribution of all samples measured in the amplitude-sweep tests. To account for the large spread in critical strains, a strain amplitude of 2%, which is within the lower part of the critical strain IQR, was chosen. Despite being low, this strain amplitude might have exceeded the critical strain of individual samples in the frequency-sweep test. This potential excessive loading could have changed the molecular structure of these samples and could have led to errors in the frequency-sweep test results. While the values of the storage and loss moduli differ across the subjects, all samples showed an increasing trend for the storage and loss moduli with increasing frequency. The loss modulus being lower than the storage modulus characterizes the tracheobronchial mucus as mainly elastic at a strain rate of 2%. Outliers underline a wide scatter between individuals.

The novel transient rheological testing of human tracheobronchial mucus gives a statistically based insight into the interplay of viscous and elastic forces over time. Transferring these

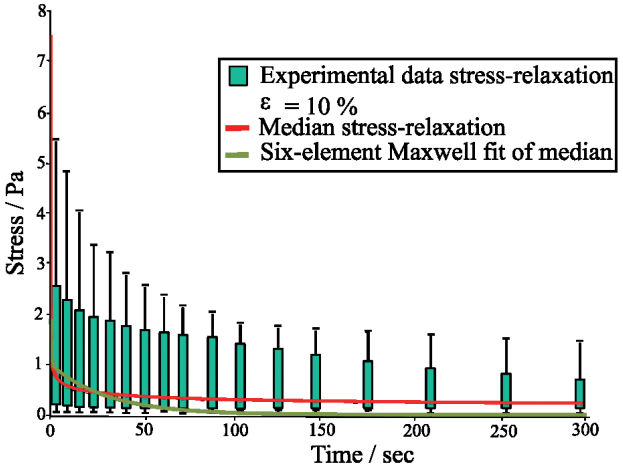

Figure 9. Stress results of stress-relaxation tests. The red line connects the median stress value at each timestep. The green line shows the stress curve predicted by the six-element Maxwell model fitted to the median stress values at each timestep.

results into mathematical models provides a basis for detailed investigations of flow phenomena in the human respiratory system such as mucus behavior during coughing or ciliary beating. Due to the variety of loads placed on the samples during the transient test, numerical models for a multitude of calculations could be deducted. Now, numerical approaches for simulating mucus behavior in different respiratory events, such as breathing at rest, coughing or ciliary motion, are available. During the creep-recovery tests at a constant stress load of 5 Pa, the mucus samples exhibited strain response curves that are characteristic for a viscoelastic fluid. At the onset of loading in the creep part of the test, a small amount of pure elastic deformation is seen in the nearly vertical strain increase. The following non-linear strain increase shows the viscoelastic behavior. Once the strain increase rate stabilizes to a constant value, the strain response is that of a pure viscous material. After the stress removal in the relaxation part of the test, the small amount of pure elastic deformation is visible in the first instantaneous strain decrease. With time, the strain decreases and settles to the non-recoverable strain caused by viscous flow. The ratios of recoverable, elastic strain to non-recoverable, viscous strain can be assessed reliably only in samples exhibiting high strain. Only a small portion of the strain is recoverable in these samples. Thus, the viscous influence has a higher impact on the viscoelastic behavior of the samples than the elastic influence. In both the creep and the recovery part of the creep-recovery test two significant outliers are visible. The constant load of 5 Pa causes a visibly higher strain in these samples. Upon load removal, these samples showed no remarkable recovery strain and a high permanent strain. Both the high strain values and the high non-recoverable strain indicate more viscous behavior in these samples. No difference in patient characteristics such as age or disease was apparent in the outlier samples. Thus, their different rheological behavior might be caused by the constant stress of 5 Pa inducing a higher strain than the critical strain of these samples. Overshooting the LVR causes permanent destruction in the mucus microstructure which affects its rheological properties. The Burgers model and the Weibull distribution represent the experimental data of the creep-recovery-tests well. The individual models and the models fitted to the median of the data at all measured frequencies have high coefficients of determination R^2 of 0.99. Thus, these models predict the mucus rheological behavior appropriately.

In the stress-relaxation test, the stress in the material decreases swiftly after loading the sample with a constant strain of 10%. The median stress settles at a low constant equilibrium stress of 0.4 Pa. Both these aspects indicate small molecules in the mucus microstructure, which can flow and relocate upon loading to decrease tension. The six-element Maxwell model approximation of the time-dependent stress response withing the stress-relaxation test showed visible differences to the experimental data. The stress predicted by the model falls below zero after 200 s. Thus, the model does not correctly predict the experimentally measured equilibrium stress. While this study focusses on physiological tracheobronchial mucus, further investigations of pathological changes in mucus's rheology will be conducted. For these studies, an even larger sample size, due to the high number of excluded samples, needs to be investigated.

Conclusions

In the present study, we assessed the steady as well as the time-dependent mechanical behavior of native tracheobronchial mucus. With a focus on the reliability of sample collection and on data reproducibility, the rheological behavior was characterized using amplitude-sweep, frequency-sweep, creep-recovery, and stress-relaxation tests. The amplitude-sweep test delivered an approximated critical strain. In frequency-sweep tests, the mucus was characterized as being mainly elastic. In transient tests, the averaged behavior as a response to deformation and force loading was investigated and approximated by common mathematical rheological models. Both the Burgers model of constant stress loading and the Weibull model of constant stress load removal show an appropriate approximation of the viscoelastic behavior of physiological tracheobronchial mucus. The six-element Maxwell model differs remarkably from the experimental data of stress-relaxation tests. With these results, we provide numerical models of the viscoelasticity of the physiological human tracheobronchial mucus. All model parameters are summarized in Tables 2 to 4. These models together with known forces or deformations can be used to simulate mucus flow in the respiratory system. Ultimately, the new numerical models enable realistic calculations of mucus flow during respiratory events such as breathing or coughing. This can improve our understanding of more complex flow phenomena such as pathogen transport or shear-induced aerosol generation. Further, it can provide insights into the mechanisms of respiratory diseases, aid in the development of new diagnostic tools and treatments, and thus ultimately improve patient outcomes.

Acknowledgements

This work is supported by the Regensburg Center of Health Sciences and Technology (RCHST), by the Bavarian Academic Forum (BayWISS) and by the Initiative and Networking Fund of the Helmholtz Association of German Research Centers (HGF) under the CORAERO project (KA1-Co-06). Special thanks go to Ulrich Schultheiss as well as to the colleagues from the center NanoChem of the Regensburg University of Applied Sciences.

References

1. Rajendran RR, Banerjee A. Mucus transport and distribution by steady expiration in an idealized airway geometry. Med Eng Phys 2019;66:26-39.
2. Lillehoj ER, Kim KC. Airway mucus: its components and function. Arch Pharm Res 2002;25:770-80.
3. Widdicombe JG. airway surface liquid: concepts and measurements. In: D.F. Rogers, M.I. Lethem, Editors. Airway mucus: basic mechanisms and clinical perspectives. Basel: Birkhäuser; 1997. p. 1-17.
4. Fahy JV, Dickey BF. Airway mucus function and dysfunction. N Engl J Med 2014;23:2233-47.
5. Martinez-Rivera C, Crespo A, Pinedo-Sierra C, Garcia-Rivero JL, Pallares-Sanmartin A, Marina-Malanda N et al. Mucus hypersecretion in asthma is associated with rhinosinusitis, polys and exacerbations. Respir Med 2018;135:22-8.
6. Lafforgue O, Seyssiecq I, Poncet S, Favier J. Rheological properties of synthetic mucus for airway clearance. J Biomed Mater Res A 2018;109:386-96.
7. Quraishi MS, Jonas NS, Mason J. The rheology of nasal mucus: a review. Clin Otolaryngol Allied Sci 1998;5:403-13.
8. Ridley C, Thornton D. Mucins: the frontline defence of the

lung. Biochem Soc Trans 2018;46:1099-106.
9. Kesimer M, Sheehan J. Mass spectrometric analysis of mucin core proteins. Methods Mol Biol 2012;842:67-79.
10. Lai SK, Wang Y, Wirtx D, Hanes J. Micro- and macrorheology of mucus. Adv Drug Deliv Rev 2009;61:86-100
11. Boegh M, Nielsen HM. Mucus as a barrier to drug delivery – understanding and mimicking the barrier properties. Basic Clin Pharmacol Toxicol 2015;116:179-86.
12. Hwang SH, Litt M, Forsman WC. Rheological properties of mucus. Rheol Acta 1969;8:438-48.
13. Zayas G, Chiang MC, Wong E, MacDonald F, Lange C, Senthilselvan A, et al. Cough aerosol in healthy participants: fundamental knowledge to optimize droplet-spread infectious respiratory disease management. BMC Pulm Med 2021;12:11.
14. Silberg A. On mucociliary transport. Biorheology 1990;27:295-307.
15. Elizer N, Sadé J, Silberg A, Nevo AC. The role of mucus in transport by cilia. Am Rev Respir Dis 1970;102:48-52.
16. Hill D, Long R, Kissner W, Atieh E, Garbarine IC, Markovets M, et al. Pathological mucus and impaired mucus clearance in cystic fibrosis patients result from increased concentration, not altered pH. Eur Respir J 2018;52:1801297.
17. Ren S, Wang L, Shi Y, Cao M, Hao L, Luo Z et al. Numerical analysis of airway mucus clearance effectiveness using assisted coughing techniques. Sci Rep 2020;10:2030.
18. Ren S, Cai M, Shi Y, Luo Z, Wang T. Influence of cough airflow characteristics on respiratory mucus clearance. Phys Fluids 2022;34:41911.
19. Taylor C, Pearson J, Draget K, Dettmar P, Smidsrod O. Rheological characterisation of mixed gels of mucin and alginate. Carbohydr Polym 2014;59:189-95.
20. Hamed R, Fliegel J. Synthetic tracheal mucus with native rheological and surface tension properties. J Biomed Mater Res A 2014;102:1788-98.
21. App EM, Zayas JG, King M. Rheology of mucus and transepithelial potential difference: small airways versus trachea. Eur Respir J 1993;6:67-75.
22. Jeanneret-Grosjean A, King M, Michoud MC, Liote H, Amyot R. Sampling technique and rheology of human tracheobronchial mucus. Am Rev Respir Dis 1988;137:707-10.
23. Atanasova KR, Reznikov LR. Strategies for measuring airway mucus and mucins. Respir Res 2019;20:261.
24. Tanaka E, van Eijden T. Biomechanical behavior of the temporomandibular joint disc. Crit Rev Oral Biol Med 2003;14:138-50.
25. Gebrehiwot SZ, Espinosa-Leal L. Characterising the linear viscoelastic behaviour of an injection moulding grade polypropylene polymer. Mech Time-Depend Mater 2021;26:791-814.
26. Imane B, Kyoungtae K, Shahab RK, Sahukhal GS, Mohamed OE, Joshua UO. Creep, recovery, and stress relaxation behavior of nanostructured bioactive calcium phosphate glass-POSS/polymer composites for bone implants studied under simulated physiological conditions. J Biomed Mater Res B Appl Biomater 2019;107:2419-32.
27. Monticeli F, Ornaghi H, Neves R, Cioffi M. Creep/recovery and stress-relaxation tests applied in a standardized carbon fiber/epoxy composite: Design of experiment approach. J Strain Anal Eng Des 2020;55:109-17.
28. Chae SH, Zhao J, Edwards D, Ho PS. Characterization of the viscoelasticity of molding compounds in the time domain. J Electron Mater 2010;39:419-25.
29. Jory M, Bellouma K, Blanc C, Casanellas L, Petit A, Reynaud P, et al. Mucus microrheology measured on human bronchial epithelium culture. Front Phys 2019;7:19.
30. Wereley N, Chaudhuri A, Yoo J, John S. Bidisperse magnetorheological fluids using fe particles at nanometer and micron scale. J Intell Mater Syst Struct 2006;17:393-401.

Received for publication: 6 June 2023. Accepted for publication: 30 August 2023.

Multidisciplinary Respiratory Medicine 2023; 18:923
doi:10.4081/mrm.2023.923